Received: 31 July 2021 | Revised: 20 September 2021 | Accepted: 27 September 2021

DOI: 10.1002/agt2.130

Aggregate Open Access WILEY

RESEARCH ARTICLE

Lanthanide-based bulky counterions against aggregation-caused quenching of dyes in fluorescent polymeric nanoparticles

Caterina Severi[1] | **Satu Lahtinen**[2] | **Jaana Rosenberg**[2] | **Andreas Reisch**[1] | **Tero Soukka**[2] | **Andrey S. Klymchenko**[1]

[1] Laboratoire de Biophotonique et Pathologies, Faculté de Pharmacie, UMR 7021 CNRS, Université de Strasbourg, Cedex, Illkirch, France

[2] Department of Biotechnology, University of Turku, Turku, Finland

Correspondence
Andrey S. Klymchenko, Laboratoire de Biophotonique et Pathologies, Faculté de Pharmacie, UMR 7021 CNRS, Université de Strasbourg, 74, Route du Rhin, 67401 Cedex, Illkirch, France.
Email: andrey.klymchenko@unistra.fr

Funding information
European Research Council ERC Consolidator grant BrightSens, Grant/Award Number: 648528

Abstract

Dye-loaded polymeric nanoparticles (NPs) are promising bioimaging agents because of their available surface chemistry, high brightness, and tunable optical properties. However, high dye loadings can cause the aggregation-caused quenching (ACQ) of the encapsulated fluorophores. Previously, we proposed to mitigate the ACQ inside polymeric NPs by insulating cationic dyes with bulky hydrophobic counterions. In order to implement new functionalities into dye-loaded NPs, here, we extend the concept of bulky counterions to anionic lanthanide-based complexes. We show that by employing Gd-based counterions with octadecyl rhodamine B loaded NPs at 30 wt% versus polymer, the fluorescence quantum yield can be increased to 10-fold (to 0.34). Moreover, Gd-anion provides NPs with enhanced contrast in electron microscopy. A combination of a luminescent Eu-based counterion with a far-red to near-infrared cyanine 5 dye (DiD) yields Forster resonance energy transfer NPs, where the UV-excited Eu-based counterion transfers energy to DiD, generating delayed fluorescence and large stokes shift of ~340 nm. Cellular studies reveal low cytotoxicity of NPs and their capacity to internalize without detectable dye leakage, in contrast to leaky NPs with small counterions. Our findings show that the aggregation behavior of cationic dyes in the polymeric NPs can be controlled by bulky lanthanide anions, which will help in developing bright luminescent multifunctional nanomaterials.

KEYWORDS
aggregation-caused quenching, dye-loaded polymeric nanoparticles, fluorescence microscopy

INTRODUCTION

Fluorescent nanoparticles (NPs) have emerged as powerful biosensing and bioimaging tools due to their superior optical properties with respect to organic dyes, while their available surface chemistry allows combining different functionalities in one theranostic platform.[1–4] There are several different types of fluorescent NPs, with the most famous being quantum dots (QDs),[5,6] dye-doped silica nanoparticles,[7] and carbon dots.[8,9] On the other hand, NPs assembled exclusively of organic materials have also gained a large interest,[10] with systems such as aggregation-induced emission (AIE) NPs,[11–13] conjugated polymer NPs[14,15] as well as dye-loaded lipid,[16] and polymer NPs,[17–19] progressively becoming more popular and widespread.

Among all the previously mentioned nanoparticle types, dye-loaded polymeric nanoparticles are attractive systems for various reasons: (i) the polymeric matrix can be designed to be biodegradable and biocompatible; (ii) it is possible to coencapsulate dyes with other contrast agents and/or drugs; (iii) the wide variety of organic dyes available makes it possible to prepare fluorescent NPs with virtually any spectroscopic characteristics.[20–24] However, at high concentrations fluorophores tend to aggregate, giving rise to the aggregation-caused quenching phenomenon (ACQ), limiting the overall brightness of the system.[18] This issue has been tackled with different approaches: the most popular and straightforward one is the use of AIE molecules.[11–13,17,25,26] It was also demonstrated that the incorporation of long hydrocarbon chains and/or bulky side groups can mitigate the ACQ

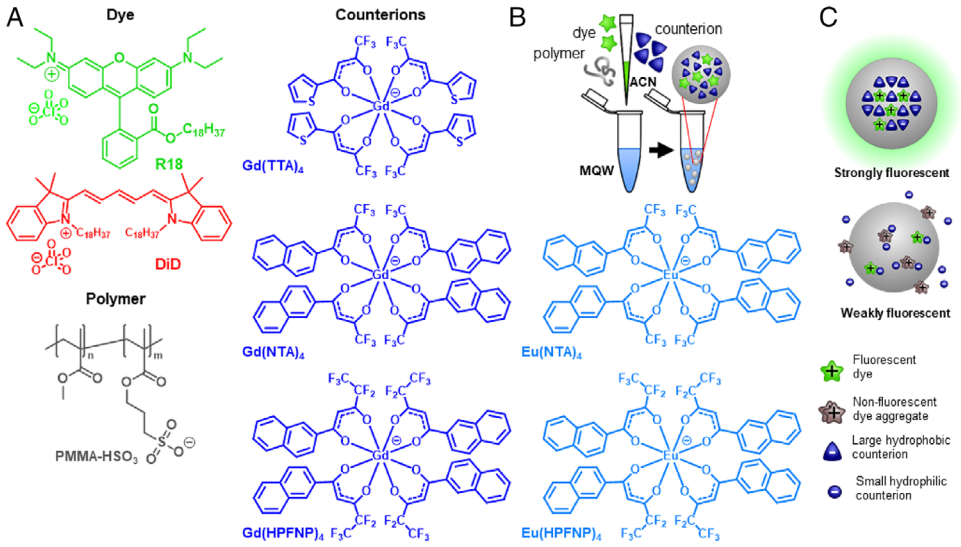

FIGURE 1 Dyes and counterions used for the preparation of dye-loaded polymeric NPs. (A) Cationic fluorescent dyes: R18 (in green), DiD (in red); sulfonate bearing polymer (in gray), and lanthanide-based anions (in blue and light blue) used for nanoparticle preparation. (B) Preparation of NPs via nanoprecipitation scheme. (C) Hypothetic models of fluorescent dye distribution inside polymeric NPs when prepared with small hydrophilic counterion perchlorate (left) and BHC (right)

phenomenon in different organic nanostructures.[27–29] In addition, when dealing with charged dyes, a powerful approach is the use of bulky hydrophobic counterions (BHC),[21,30] which insulate the fluorophores effectively to avoid ACQ and at the same time improve the dye encapsulation inside the polymeric matrix, thus preventing dye leaching in biological media. These counterions belong to the class of weakly coordinating anions due to their large size and delocalization of charge.[31] Notable examples are fluorinated tetraphenylborates (TPBs), tetraalcoxyaluminates, bis(alkylsulfonyl)-imides, etc. Weakly coordinating ions found a broad range of applications ranging from catalysis,[32] electrochemistry,[33] ionic liquids,[34,35] lithium batteries,[36] ion sensors,[37] and organic light-emitting diodes.[38] Owing to their capacity to control aggregation of cationic dyes, BHC found yet another application in the formulation of dye-loaded polymeric nanoparticles,[21,30] ultra-small fluorescent micelles,[39] and ultrabright dye-counterion aggregates.[40–43]

Originally, the concept of bulky counterions for preventing ACQ in polymer NPs was developed based on perfluorinated tetraphenyl borate (F5-TPB).[21] Later studies showed that these counterions can be replaced by other bulky, hydrophobic, and especially fluorinated counterions based on aluminates[44] and boron hydrides.[30] In addition, supramolecular bulky counterions based on a complex of the anion with a macrocycle were also introduced for preventing the ACQ of different dyes.[45] The concept of ionic dye insulation with BHC is quite generic because it is applicable to different cationic rhodamines[46] and cyanines.[20,47] It enabled the preparation of polymeric NPs in the size range of 10–40 nm with brightness 100-fold higher than corresponding QDs.[48,49] They enabled single-particle tracking both in vitro inside cells[50,51] as well as in vivo in mice brains.[52] Moreover, counterion ensures close proximity of dyes inside polymeric NPs, which induces ultrafast dye–dye energy transfer generating giant light-harvesting nanoantenna that amplifies ~1000 fluorescence signal through Forster resonance energy transfer (FRET).[53] The latter has already been applied to amplified FRET-based detection of nucleic acids[49,54,55] and oxygen.[47] However, in all these previous works, the counterion function was focused on preventing ACQ and dye leaching; while, theoretically, it could be possible to tailor the structure of the counterion in order to implement new functions into the nanomaterials.

In this work, we further extended the library of bulky counterions by testing a family of lanthanide (gadolinium and europium) chelated counterions with increasing hydrophobicity (Figure 1A). Lanthanide-based nanomaterials found wide usage in theranostics applications due to their unique spectroscopic properties, such as many narrow emission bands, long lifetimes, background-free X-ray-excited luminescence, and potentially upconversion.[56–58] In the specific context of dye-loaded polymeric nanoparticles, the reasons behind preparing NPs loaded with lanthanide-based counterions are multiple: (i) lanthanides are heavy atoms routinely used as contrast agents in transmission electron microscopy (TEM); therefore, dye-loaded fluorescent nanoparticles encapsulating a lanthanide-based counterion can function as multifunctional platforms for fluorescence microscopy and TEM; (ii) europium complexes are attractive luminescent reporters due to their long-lived emission,[59–61] allowing background-free time-gated luminescence biosensing[62–65]; (iii) emission bands of the UV-excited europium complexes fall in the visible, making it a potential FRET donor for the cationic fluorescent dyes coupled with such counterion, generating ultra-long Stokes shift systems. We tested these lanthanide-based counterions by formulating NPs loaded with two cationic dyes: an octadecyl ester of rhodamine B (R18) and a dioctadecyl derivative of cyanine 5 (DiD) (Figure 1A). NPs prepared with Gd-based counterions featured superior quantum yields (QY), smaller sizes, and narrower emission bands with respect to NPs prepared with R18 perchlorate and DiD perchlorate. Moreover, when imaged by TEM they displayed a strong contrast with respect to NPs formulated without heavy atom-based counterions. When an ion pair of cationic DiD with anionic europium complexes were used for encapsulation, we

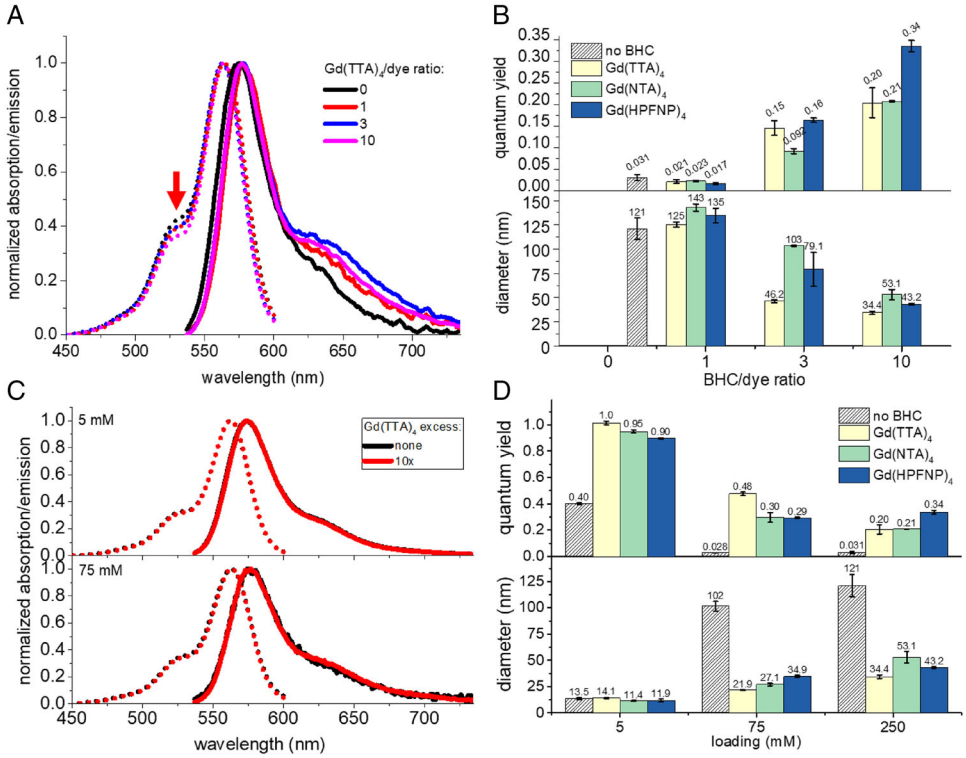

FIGURE 2 Characterization of PMMA-MA NPs loaded with R18 and Gd-based counterions. (A) Normalized absorption and emission spectra of NPs formulated with R18 (250 mM with respect to the polymer) and increasing quantities of $Gd(TTA)_4$, the red arrow highlights a decreasing of the absorption spectrum shoulder upon the increase of $Gd(TTA)_4$/dye ratio. (B) Fluorescence QY (top) and particle size (bottom) as a function of counterion/dye molar ratio for each counterion (λ_{exc} = 535 nm). (C) Normalized absorption and emission spectra of NPs loaded with R18 (5 and 75 mM) without BHC or with a 10-fold excess of $Gd(TTA)_4$. (D) Fluorescence QY (top) and particle size (bottom) for R18-loaded NPs as a function of dye loading with and without a 10-fold excess of each Gd-based counterion (λ_{exc} = 535 nm)

obtained an efficient FRET from the lanthanide anion to the cationic dye generating delayed fluorescence with ~340 nm Stokes shift. Cellular studies showed that the dye/Gd-anion loaded NPs readily internalized by endocytosis with little to no leaching of the fluorescent dye, while NPs prepared in the absence of the bulky counterion displayed a marked dye leaching behavior. Finally, the NPs loaded with dye paired with the lanthanide anion displayed minimal cytotoxicity at concentrations habitually used for cellular imaging.

RESULTS AND DISCUSSION

Preparation of NPs based on lanthanide counterions

To design the lanthanide counterions, we used Gd and Eu salts, known to yield optically transparent and emissive complexes, respectively. For the Gd ion, we prepared three complexes characterized by increasing size and/or fluorination level in the following order: $Gd(TTA)_4$ < $Gd(NTA)_4$ < Gd(HPFNP) (Figure 1A), based on previous reported synthetic protocols.[66] For the Eu ion, the two largest complexes were prepared: $Eu(NTA)_4$ and Eu(HPFNP). First, we attempted to prepare pure salts of R18 dye with corresponding lanthanide-based counterions (Figure 1A) by ion exchange followed by silica gel chromatography, following previously reported protocol for F5-TPB counterions.[20,21] However, the dye salts showed a tendency to decompose on silica. We suspect that lanthanide-based counterions are not as hydrophobic as fluorinated TPB (e.g. F5-TPB) so that they undergo an ion exchange on the silica. Therefore, we mixed the dye perchlorate salt with the lanthanide-based counterion potassium salt in organic solvent and used this mixture to formulate polymeric NPs. The latter was obtained by charge-controlled nanoprecipitation[67] of poly(methyl methacrylate) (PMMA-MA) polymer in a buffer from acetonitrile containing both polymer and the mixture of the dye with the lanthanide complex.

First, we investigated the optimal ratio between the dye and the BHC counterion in the formulation of NPs. To this end, PMMA-MA NPs were loaded with 250 mM of R18 with respect to the polymer and varied quantities of Gd-based BHC (Figure 1A), and then their sizes and spectroscopic properties were evaluated (Figure 2). It was immediately clear that NPs formulated with R18 perchlorate in the absence of BHC tended to yield poorly emissive particles due to ACQ. Moreover, according to the dynamic light scattering (DLS), their size was much higher than that observed for blank PMMA-MA NPs (~50 nm).[48] The latter suggested that the dyes were not properly encapsulated, resulting in relatively large particle aggregates (Figure 1C), in line with previous studies.[21,30]

Preparing NPs with a dye/BHC molar ratio 1:1 improved neither the QY nor the particle size (Figure 2B). A threefold excess of BHC marginally increased the QY of the NPs and yielded smaller sizes, while NPs formulated with a 10-fold excess of BHC yielded NPs with very high QY (up to 0.34) and the smallest size for all three tested Gd-BHC. For the highest dye loading (250 mM vs. polymer), we observed that

the presence of higher quantities of Gd-BHC in the polymeric matrix also had an effect on absorption spectra (Figure 2A), with the short-wavelength shoulder intensity decreasing with the increase in Gd-BHC loading. Indeed, for NPs without BHC, the absorbance ratio between the shoulder and the maximum peak was 0.42. For $Gd(TTA)_4$/dye ratios of 1 and 3, the contribution of the shoulder decreased to 0.39 and at 10-fold excess of $Gd(TTA)_4$ further dropped to 0.37. Overall, this decrease of the height of the shoulder is an indication of a lower degree of dye aggregation in the presence of the counterion.[30]

It should be noted that the BHC/dye ratios employed in these NP formulations (feed ratios) do not necessarily reflect the actual BHC/dye ratio in the formed NPs. We measured the actual BHC/dye ratio inside NPs by quantifying the absorption spectra of samples before and after dialysis versus release medium containing β-cyclodextrin (Supplementary Figure S1), according to the previously developed method.[30,44] The actual BHC/dye ratios were found systematically lower than the feed ratio: for the feed BHC/dye ratio of 10, the actual ratio after dialysis was 3.7 for $Gd(TTA)_4$, and 6.1–6.2 for $Gd(NTA)_4$ and $Gd(HPFNP)_4$ (Supplementary Figure S2A). The observed higher actual ratios for $Gd(NTA)_4$ and $Gd(HPFNP)_4$ compared to that for $Gd(TTA)_4$ correlate well with their higher hydrophobicity. Together with the spectroscopy data, these results suggest that excess of Gd-BHC is necessary to displace all perchlorate anions, in order to prevent ACQ of R18 in the polymer matrix of NPs.

Dialysis experiments also allowed us to estimate the encapsulation efficiency of R18 dye. In line with previous studies,[30,44] we observed a poor degree of dye encapsulation for NPs formulated with R18 perchlorate (Supplementary Figure S2B). In sharp contrast, introducing a BHC rendered the R18 dye encapsulation efficiency nearly quantitative for all studied BHC/dye ratios (Supplementary Figure S2B), suggesting a crucial role of La-counterions for efficient dye encapsulation, in line with the previous study on fluorinated TPBs.[30]

Effects of dye loading

After establishing that the optimal BHC molar excess versus R18 was 10-fold, we proceeded to test different loadings of R18 with and without the 10-fold excess of different Gd-BHC. At the lowest loading (5 mM), there was no marked effect of counterion on particle size because the dye concentration was too low to influence the particle formation process (Figure 2D). However, there was a strong effect on fluorescence QY, with an increase from 0.4 to > 0.9 in the presence of Gd-BHC. This result is a clear indication that even at very low loading R18 shows a marked tendency to aggregate inside the polymeric matrix. The dye aggregation was further supported by an observed significantly higher short-wavelength shoulder in absorption spectra of R18-only NPs compared to that of the dye in EtOH (Supplementary Figure S3A).

At the intermediate loading of R18 (75 mM), there was a marked effect on both particle size and fluorescence QY, where $Gd(TTA)_4$ performed best, both in terms of QY and size (0.48 and 22 nm). However, at the highest loading (250 mM), the trend inverted, and the highest QY was obtained by employing the largest counterion $Gd(HPFNP)_4$ (Figure 2D). The latter NPs displayed a QY of 0.34, which is close to that of PMMA-MA NPs loaded with R18 and fluorinated TPB F5-TPB (our benchmark counterion).[53] In contrast, the situation was different without BHC: at intermediate and high loadings, the QY of R18 perchlorate was 0.028–0.031, indicating strong ACQ. Our previous studies showed that in the absence of bulky fluorinated counterions (e.g., using nonfluorinated TPB), the mean fluorescence lifetime drops dramatically at higher dye loading, in contrast to bulky fluorinated counterion F5-TPB. These much lower lifetime values indicate that that ACQ of R18 is associated with fast nonradiative deactivation processes in the dye aggregates. The capacity of Gd-BHC to prevent ACQ is clearly related to their much larger size compared to perchlorate used in parent R18 dye. Indeed, the radius of $Gd(TTA)_4$ anion is ~1 nm[68] versus 0.24 nm for perchlorate.[69] This implies that the difference in their diameter and thus the distance between the π–π planes of the dyes is increased by ~1.5 nm with BHC, which can explain their effect against ACQ.

We compared the brightness of our system with quantum dots (QD585), luminescent nanoparticles with a CdSe semiconductor core, which have been extensively used in bioimaging due to their exceptional brightness and photostability.[5,6] Taking into account the number of encapsulated dyes (n), the extinction coefficient of each dye (ε), and the QY, we can estimate the brightness (B) of each dye-loaded NP sample using the equation $B = n \times \varepsilon \times QY$.[18] The number of encapsulated dyes can be calculated from the volume of the NPs (obtained from the DLS diameters assuming spherical shape) and the loading of dye in the polymeric matrix. For NPs loaded with R18/$Gd(TTA)_4$ (250 mM): $B = 2800 \times 125{,}000\ M^{-1}\ cm^{-1} \times 0.20 = 7 \times 10^7\ M^{-1}\ cm^{-1}$, which is roughly equivalent to ~226 QD585 ($B = 3.1 \times 10^5$ $M^{-1}\ cm^{-1}$, with excitation at 532 nm, assuming that QY = 1). For R18/$Gd(NTA)_4$ $B = 10200 \times 125{,}000\ M^{-1}\ cm^{-1} \times 0.21 = 2.5 \times 10^8\ M^{-1}\ cm^{-1}$, roughly equivalent to ~800 Qdots 585. While for NPs R18/$Gd(HPFNP)_4$ (250 mM) $B = 5500 \times 125{,}000\ M^{-1}\ cm^{-1} \times 0.43 = 3 \times 10^8\ M^{-1}\ cm^{-1}$, roughly equivalent to ~1000 QD585. We should note that the differences would be less dramatic if Qdots 585 are excited in the violet region (e.g., 405 nm), where it is expected to show a 10-fold higher absorption coefficient. Moreover, the hydrodynamic dimers of QD585 are smaller (20–25 nm) than PMMA-MA studied here (34–53 nm).

Transmission electronic microscopy

TEM was done for NPs at the three different R18 dye loadings (5, 75, and 250 mM) formulated with a 10-fold excess of $Gd(TTA)_4$ as well as NPs loaded with 250 mM R18 together with $Gd(NTA)_4$ and $Gd(HPFNP)_4$ counterions (Figure 3). It should be noted that TEM size analysis mostly reproduced the results obtained with DLS, with the only exception of R18/ $Gd(TTA)_4$ (250 mM). The reason for the latter is unclear, but it might be due to the process of immobilization on the TEM grid, which can compromise the stability of NPs. Moreover, it should be noted that the Gd-loaded NPs could be readily detected via TEM without the use of any contrast agent, while control NPs without Gd-BHC were noticeably less visible (Figure 3). This implies that heavy Gd-atoms

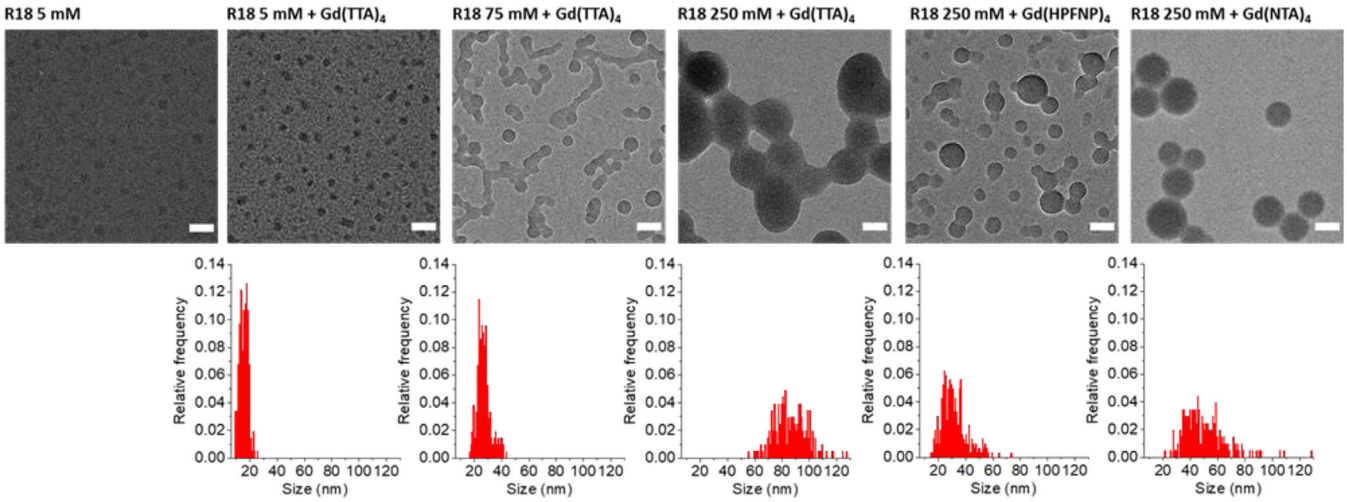

FIGURE 3 TEM images of R18-loaded PMMA-MA NPs with different Gd-based counterions in a 10-fold excess (top) and relative size distributions (bottom). Scale bars: 50 nm

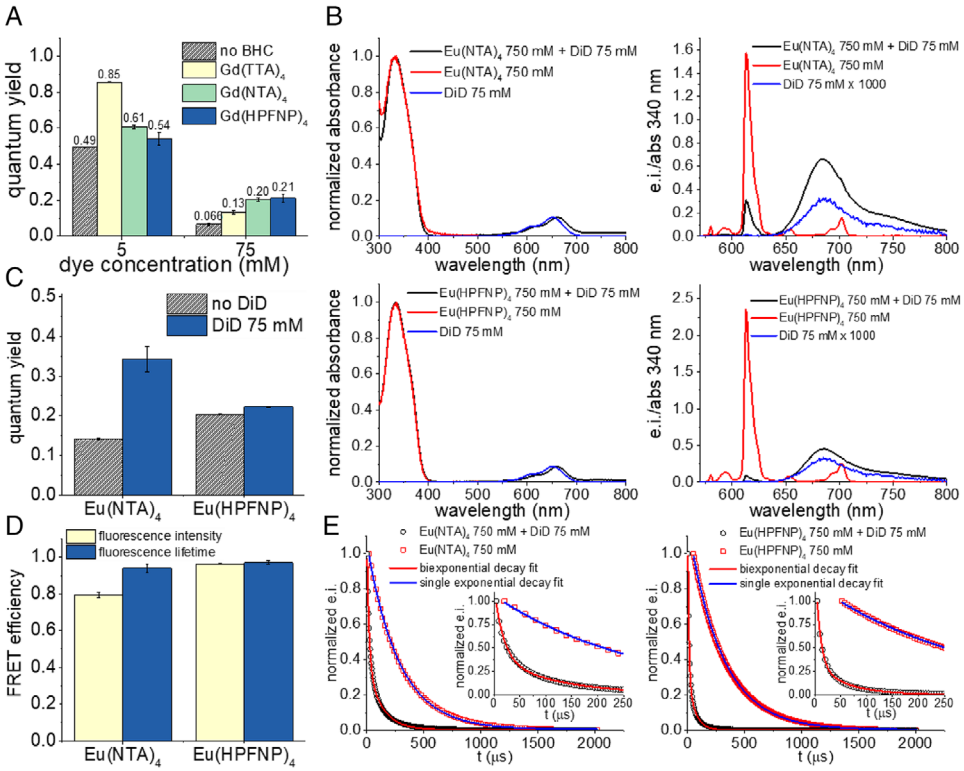

FIGURE 4 FRET NPs loaded with DiD and Eu-based counterion. (A) Fluorescence QY for NPs at different DiD loadings formulated with and without a 10-fold excess of each Gd-based counterion. (B) Absorption (left) and emission (right) spectra for FRET and control nanoparticles formulated with DiD at a loading of 75 mM and a 10-fold excess of $Eu(NTA)_4$ (top) and $Eu(HPFNP)_4$ (bottom) (for FRET and donor-only NPs: λ_{exc} = 340 nm, for DiD-only NPs: λ_{exc} = 620 nm). (C) QY of $Eu(NTA)_4$ and $Eu(HPFNP)_4$ nanoparticles with and without acceptor. (D) FRET efficiency of FRET NPs calculated from fluorescence intensity and fluorescence lifetime. (E) Fluorescence decay curves for $Eu(NTA)_4$ NPs (left) and $Eu(HPFNP)_4$ NPs (right) with and without DiD

could improve TEM contrast so that the combination of dye with Gd-BHC could enable bimodal imaging combining TEM and fluorescence techniques.

Encapsulation of cyanine 5 dye and FRET from Eu-BHC

Next, we tested whether Gd-BHC can prevent ACQ of another cationic dye—cyanine 5 derivative DiD (Figure 1A), operating in a far-red to near-infrared region.[70,71] At low loading (5 mM), the same trend as for R18 was reproduced, with a strong increase in QY (from 0.49 to 0.85), $Gd(TTA)_4$ performing the best, and $Gd(HPFNP)_4$ performing the worst (Figure 4A). As previously observed for the R18 dye, DiD perchlorate also displayed a tendency to aggregate inside the polymeric matrix even at low loadings (Supplementary Figure S3B). At the highest loading investigated with DiD (75 mM), again the trend inverted, with $Gd(TTA)_4$ yielding the lowest QY (0.13) among the three tested Gd-BHC and $Gd(HPFNP)_4$ showed the best QY (0.21). Thus, for two cationic dyes R18 and DiD of different colors

and dye families, we found that at the highest loading the bulkiest counterion Gd(HPFNP)$_4$ provides the best dye insulation against ACQ. Thus, the bulkiest BHC provides the best spacing/insulation of the cationic dyes, which ensures their minimal ACQ in the polymeric NPs at the high loading (i.e., local concentration). Moreover, according to fluorescence correlation spectroscopy (the sample was incompatible with DLS laser at 633 nm), the hydrodynamic diameter of DiD-loaded NPs significantly decreased in the presence of BHCs, similarly to R18-loaded NPs (Supplementary Figure S4).

The most interesting aspect of formulating DiD-loaded NPs was in constructing a FRET system where Eu-based BHC function as donors and DiD as acceptor. Eu ions display many narrow emission bands in the visible,[60,61] its strongest one overlapping very well with DiD absorption. Moreover, owing to its aromatic ligands the Eu complexes strongly absorb in the UV. Therefore, the ion pair with DiD could undergo FRET, yielding a system with a quite large Stokes shift, absorbing in the UV to emit in the far red.

We formulated FRET NPs comprising 75 mM of DiD (acceptor) and a 10-fold molar excess (i.e.,750 mM) of Eu-BHC (donor). Control NPs loaded with only donor or only acceptor were also formulated. We found that when exciting the Eu-BHC (at 340 nm) the FRET NPs displayed a strong acceptor emission and relatively weak donor bands, while at the same concentration donor-only NPs showed much stronger donor emission (Figure 4B). Acceptor-only NPs, when excited at 340 nm, showed a negligible emission, three orders of magnitude weaker than that of the FRET NPs, meaning that the contribution of direct excitation of the acceptor is negligible in the FRET NPs. NPs formulated with Eu(HPFNP)$_4$ displayed a higher QY with respect to NPs formulated with Eu(NTA)$_4$ (Figure 4C). When introducing the acceptor, the total QY of the system improved for both BHC, but more significantly for Eu(NTA)$_4$, almost doubling in value (Figure 4C).

Moreover, we recorded the time-resolved fluorescence decay curves of donor-only NPs and FRET NPs at an emission wavelength of Eu (Figure 4E) and calculated their lifetimes. We found that donor only NPs displayed a single exponential decay, with NPs loaded with K[Eu(NTA)$_4$] having a lifetime of 281 $\pm$ 1 μs and NPs loaded with K[Eu(HPFNP)$_4$] having a lifetime of 296 $\pm$ 1 μs. On the other hand, FRET NPs displayed a biexponential decay, meaning that the system had two different lifetimes (18.0 $\pm$ 0.3 and 127 $\pm$ 2 μs for NPs with Eu(NTA)$_4$ as a donor; 9.2 $\pm$ 0.1 and 61 $\pm$ 1 μs for NPs with Eu(HPFNP)$_4$ as donor). The lifetime with the largest amplitude was the shortest. This means that not all Eu-BHC transfer efficiently their excitation energy, with only a minor fraction of Eu-based complexes having a longer lifetime. Remarkably, a time-gated emission spectrum of NPs loaded with DiD and Eu(HPFNP)$_4$ after 100 μs delay still showed a significant contribution of DiD emission, centered at 682 nm (Supplementary Figure S5). As at this time delay, one should not expect any emission of DiD (~3 ns lifetime in PMMA-MA NPs[53]) originated from the direct excitation, we can conclude that this long-wavelength band corresponds to the delayed emission generated by FRET from the Eu(HPFNP)$_4$ donor to the DiD acceptor.

We further measured FRET efficiency using both fluorescence emission and the lifetime of the donor. For NPs with Eu(HPFNP)$_4$ as the donor, the two values were in good agreement, being close to unity. The short lifetimes of the FRET NPs confirmed also that the energy transfer between the Eu-BHC and DiD is nonradiative resonance-energy transfer and not based on reabsorption of the donor emission. For Eu(NTA)$_4$ as a donor, the FRET efficiency calculated from the lifetime was higher than the value calculated from the intensity. This overestimation is probably due to the presence of a fraction of BHC that has a longer lifetime. Aside from this, both counterions produced high FRET efficiency, with Eu(HPFNP)$_4$ being the best performing (Figure 4D).

Single-particle measurements

Next, we studied the fluorescence properties of the prepared NPs via fluorescence microscopy. We selected the NPs with the highest R18 loading (250 mM) and a 10-fold excess of each Gd-based counterion. Their brightness was compared with QDs emitting in the same spectral window, QD585. The polymeric NPs and QDs were immobilized on a polyethyleneimine (PEI) covered glass surface and imaged with a wide-field fluorescence microscope. What we observed was in line with the spectroscopic data recorded in a cuvette. All polymeric NP samples were brighter than the reference QDs (Figure 5), with the brightest samples being R18/Gd(NTA)$_4$ and R18/Gd(HPFNP)$_4$. According to single-particle microscopy analysis, R18/Gd(TTA)$_4$ NPs were as bright as ~375 QD585, while R18/Gd(NTA)$_4$ and R18/Gd(HPFNP)$_4$ displayed brightness of ~1300 QD585, in accordance with our theoretical estimations. Thus, our single-particle analysis data confirms that the largest counterions yield the brightest NPs, probably due to the best dye insulation inside NPs.

Cellular studies

Finally, we tested our new NPs for cellular imaging experiments. NPs formulated with a 10-fold excess of each of the three Gd-BHC and without were incubated with HeLa cells for 3 h at 37°C and then imaged with a fluorescence microscope in an epi-fluorescence mode. While NPs formulated in the presence of Gd-BHC were internalized by endocytosis (observed as dots in the perinuclear region) with no sign of dye leaching, R18 NPs showed a marked leaching behavior with the dye staining the whole cell. This is in line with previous observations, wherein the absence of a BHC, the fluorescent dye was not well encapsulated in the particle and therefore tended to leach in the cellular context.[20,30] Interestingly, NPs loaded with Gd(HPFNP)$_4$, despite yielding the brightest particles in all the previous experiments, were barely visible, while Gd(TTA)$_4$ and Gd(NTA)$_4$ performed similarly well (Figure 6), whereas those with Gd(HPFNP)$_4$, despite yielding the brightest particles in all the previous experiments, were barely visible (their signal was multiplied threefold to achieve comparable contrast). Finally, we tested the cytotoxicity of NPs formulated with Gd-based counterions via the MTT assay and found no cytotoxic effect at concentrations habitually used for cellular imaging (up to 0.004 gL). However, cell viability began to decline at higher concentrations (Figure 7).

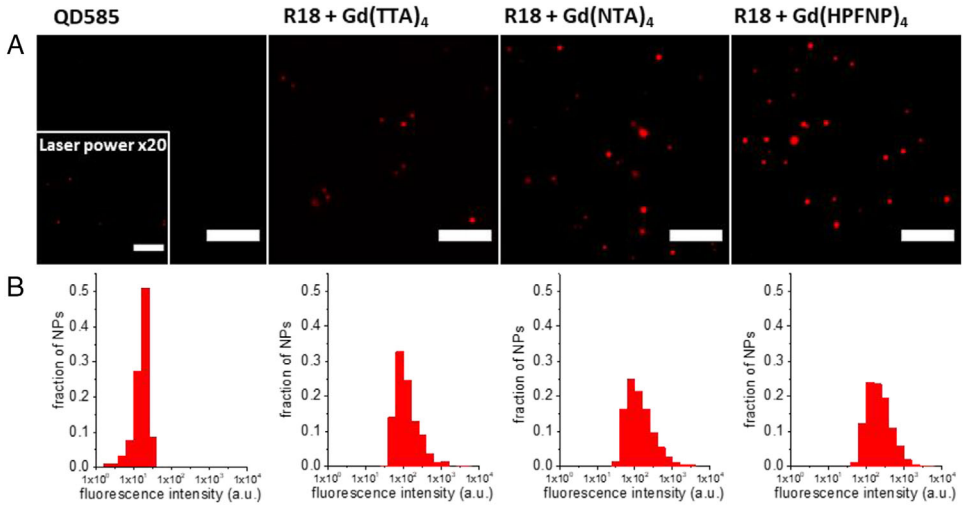

FIGURE 5 Single-particle characterization of Gd-based NPs. (A) Single-particle fluorescence images of PMMA-MA NPs prepared with a 10-fold excess of Gd-based counterion with R18 dye loading of 250 mM compared to reference quantum dots QD585. (B) Brightness histograms of the images shown in (A). Widefield microscopy was performed with excitation at 550 nm. Scale bars: 5 μm

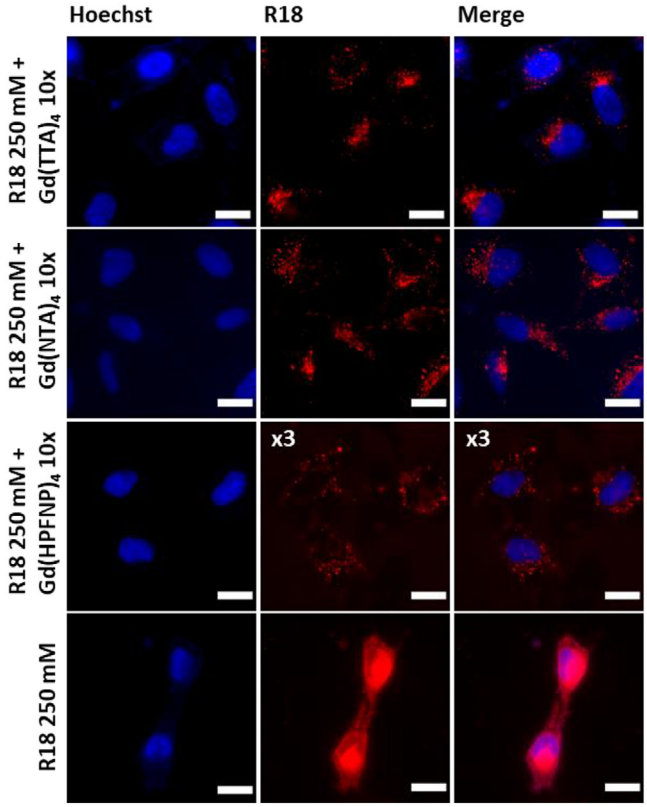

FIGURE 6 Epifluorescence microscopy images of HeLa cells incubated for 30 min at 37°C with polymeric NPs loaded with 250 mM R18 (with respect to the polymer, final R18 concentration in the medium ~1 μM) with and without a 10-fold excess of Gd-BHC. In the presence of Gd-BHC NPs get internalized by endocytosis without any dye leaching, while without the Gd-counterion there is strong leaching of the fluorescent dye. In the case of $Gd(HPFNP)_4$, the signal was multiplied by 3 (× 3) in order to achieve sufficient contrast. Scale bars: 50 μm

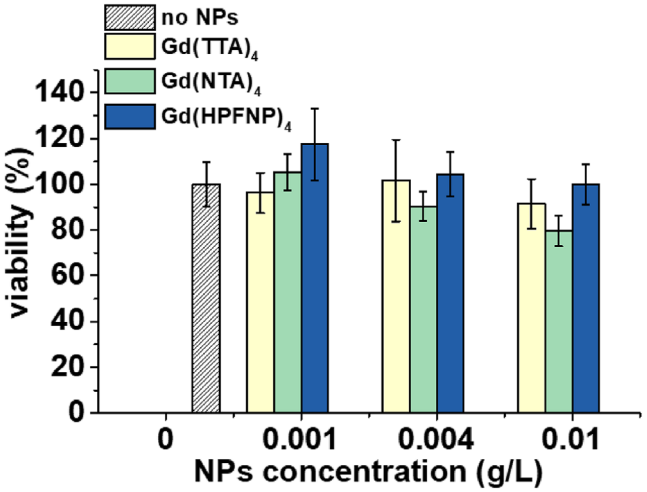

FIGURE 7 Cytotoxicity experiments for polymeric NPs loaded with 250 mM R18 + Gd-BHC 10×. The error bars represent the standard error of the mean ($n = 6$)

CONCLUSION

Bulky hydrophobic counterions enable the preparation of bright dye-loaded polymeric nanoparticles due to the dye insulation effect minimizing aggregation-caused quenching. Previously, this approach was validated on fluorinated TPBs and tetraalkoxyaluminates. In this work, we further extend this approach to yet another class of bulky anions: lanthanide complexes. NPs were prepared with three different Gd-based counterions and two different Eu-based counterions, with varied bulkiness, hydrophobicity, and fluorination level. We found that NPs loaded with Gd-based counterions showed superior QY and smaller diameters with respect to their counterparts based on small hydrophilic counterion. These positive effects were observed for both rhodamine dye R18 and cyanine dye DiD, showing that lanthanide-based counterions can be applied to different dye families. Moreover, the encapsulation of dyes with Gd-BHC provided a stronger TEM contrast with respect to control NPs. The as-prepared NPs incubated with cells could readily internalize without dye leaching, due to Gd-based counterions that ensured better dye encapsulation. MTT assays revealed the NPs to be nontoxic at the concentration used for imaging. Moreover, counterions based on Eu complexes were encapsulated with DiD and employed as FRET donors, obtaining very efficient FRET with delayed emission in the far red region upon UV

excitation, thus displaying an ultra-large Stokes shift. Our findings show that the anionic complexes of lanthanides can control the aggregation behavior of cationic dyes in a polymeric matrix, yielding bright fluorescent NPs, and potentially allow implementing additional functions due to the unique properties of lanthanides.

EXPERIMENTAL/METHODS

Materials

Methyl methacrylate (99%), 3-sulfopropyl methacrylate potassium salt (98%), acetonitrile (anhydrous, 99.8%), rhodamine B octadecyl ester perchlorate (> 98.0%), PEI (branched), potassium hydroxide (≥85%, pellets), tris(hydroxymethyl)aminomethane (ACS reagent, ≥99.8%), 2-acetonaphthone (99%), sodium hydride (90%, dry), THF (≥99.9%, anhydrous), ethyl pentafluoropropionate (98%), 4,4,4-trifluoro-1-(2-naphthyl)-1,3-butanedione (99%), 2-thenoyltrifluoroacetone (99%), europium(III) chloride (99.99%), and gadolinium(III) chloride (99.99%) were purchased from Sigma-Aldrich. MilliQ-water (Millipore) was used in all experiments. 1,1′-Dioctadecyl-3,3,3′,3′-tetramethylindodicarbocyanine perchlorate (DiD' oil) and Qdot585 streptavidin conjugate were purchased from Thermo-Fisher Scientific.

Synthesis

The polymer PMMA-HSO_3 was synthesized following a previously described procedure.[50] HPFNP was synthesized according to a previously described procedure.[66] The lanthanide-based complexes were synthesized according to a previously described procedure.[66] The ligand, either 2-thenoyltrifluoroacetone (TTA), 4,4,4-trifluoro-1-(-2-naphthyl)-1,3-butanedione (NTA) or HPFNP was dissolved in ethanol and combined with EtOH solution of KOH. Then aqueous lanthanide(III) chloride solution was added dropwise to reach the molar ratio to the ligand of 1:4 in the case of Gd(III), and 1:3.2 in the case of Eu(III). The product was precipitated with water, the precipitate was then filtered, washed twice with cold water, and dried.

Nanoparticles preparation and characterization

PMMA-HSO_3 (at a concentration of 2 mg mL^{-1}), different amounts of dye ranging from 5 mM to 250 mM (with respect to the polymer), and Gd-based counterions (where specified) were dissolved in acetonitrile. This as-prepared organic stock solution was then diluted initially in a 10-fold excess of milliQ water under shaking and then rapidly diluted a second time in a fivefold excess of milliQ water.

The encapsulation degree of R18 dye was measured through absorption spectroscopy by quantifying the dye absorption peak in the sample before and after dialysis, using a previously established protocol.[30] The actual BHC/dye ratio was measured through absorption spectroscopy by quantifying the ratio of absorbance of the counterion and dye peaks before and after the dialysis. Dialysis was performed by mixing 0.45 mL of NPs with 0.55 mL of 1 mM β-cyclodextrin solution. This solution was then dialyzed using a MEMBRACEL MD34 14V100 membrane (MWCO 14000) for 24 h with 1 mM β-cyclodextrin solution as a recipient medium. Then the solution was recovered, and its absorption spectrum was measured.

The nanoparticle diameter was determined by DLS using a Zetasizer Nano ZSP (Malvern Instruments S.A.). For the data analysis, the mean value of the size distribution per volume was taken. The nanoparticle diameter of DiD-loaded NPs was determined by fluorescence correlation spectroscopy. The measurements were performed on a custom-built confocal setup based on a Nikon Ti-E inverted microscope with a Nikon 60× 1.2NA (Tokyo, Japan) water immersion objective. Excitation was provided by a cw laser diode (638 nm, Oxxius, Lannion, France), and photons were detected through a bandpass 694/50 nm filter (Semrock, Rochester, NY, USA) with a fibered avalanche photodiode (APD SPCM-AQR-14-FC, PerkinElmer, Rodgau, Germany) connected to an online hardware correlator (ALV7000-USB, ALV GmbH, Hessen, Germany). The typical acquisition time was ∼7 min (40 × 10 s) with a nominal excitation power of 1 mW. The data were analyzed using PyCorrFit software.[72]

For the spectroscopic characterization, all the solvents used were of spectroscopic grade and MilliQ water was used in all experiments. Absorption spectra were recorded on a Cary-4000 scan UV-visible spectrophotometer (Varian), while emission spectra were recorded with a spectrofluorometer FS5 (Edinburgh Instruments). Fluorescence spectra were corrected both for lamp fluctuations and detector response. The emission spectra were recorded setting the excitation wavelength to 535 nm for R18-based NPs and at 340 nm for Eu-based NPs and at 620 nm for NPs loaded exclusively with DiD. Fluorescence QY of nanoparticles loaded with rhodamine B octadecyl ester perchlorate were calculated using Rhodamine 101 (QY = 1.0 in MeOH) as a standard[73]; for nanoparticles loaded with Eu complexes (with and without FRET acceptor), quinine sulfate (QY = 0.52 in H_2SO_4 0.05 M) was taken as a reference; while for nanoparticles loaded exclusively with DiD, Nile blue (QY = 0.27 in EtOH) was taken as a reference.[74]

Fluorescence decays of nanoparticles loaded with Eu complexes (with and without FRET acceptor) were recorded on a Cary Varian Eclipse spectrofluorometer using the lifetime mode with an excitation wavelength of 337 nm (20 nm slit) and emission wavelength 612 nm (20 nm slit). Emission lifetimes were obtained by fitting the data to single or biexponential decay function.

The FRET efficiency was calculated both from donor fluorescence intensity and lifetime using the following formulas:

$$E = 1 - \frac{I_D^A}{I_D} \quad (1)$$

$$E = 1 - \frac{\tau_D^A}{\tau_D}, \quad (2)$$

where I_D^A and I_D are the donor fluorescence intensity in the presence and absence of acceptor, respectively and τ_D^A and τ_D are the donor fluorescence lifetime in the presence and absence of acceptor, respectively.

Single-particle fluorescence microscopy

For single-particle fluorescence microscopy experiments, the NPs were adsorbed on a glass surface (LabTek 8-well plate) according to a previously described procedure.[21] The glass surface was first treated with KOH solution 1 M and subsequently incubated with a solution of PEI 1 g L^{-1} in TRIS 10 mM, pH 7.4. The NP suspensions were diluted 100 times, and they were incubated on the PEI-covered glass for 15 min before washing and measuring with a layer of milliQ water above the sample. QD585 (10 pM) was immobilized on the glass surface with the same protocol.

Single-particle measurements were performed in the wide-field epi-fluorescence more with a Nikon Ti-E inverted microscope with a 60× objective (Apo TIRF, oil, NA 1.49, Nikon). The excitation was provided by light-emitting diodes (SpectraX, Lumencor). The sample was excited at 550 nm with a LED at a power of 6.75 mW. Images were recorded with an integration time of 200 ms, and the single-particle analysis was performed on the FIJI software.

Particles were detected using a FIJI macro (available upon request) applied to a projection (average intensity) of 10 frames using an appropriate threshold: after automatic background subtraction, the mean intensities of a circular region of interest with a diameter of 6 pixels around the as-found intensity maximum were measured. Then the intensity in the circular regions of interest was integrated over the first five frames, and it was used to generate the particle intensity histograms.

Transmission electron microscopy

Five microliters of NPs suspension was deposited on carbon-coated copper-rhodium TEM grids previously treated via amylamine glow-discharge. The prepared grids were imaged using a Tecnai F20 Twin transmission electron microscope (FEI Eindhoven Holland) operating at 200 kV. Images of areas of interest were acquired with a US1000 camera (Gatan). Image analysis was performed in FIJI.

Cellular studies

HeLa cells were cultured in DMEM (Gibco-Invitrogen) supplemented with 10% FBS (Lonza), 5% L-glutamine (Gibco-Invitrogen), and 1% antibiotic solution (penicillin-streptomycin, Gibco-Invitrogen) at 37°C in a humidified atmosphere containing 5% of CO_2. Cells were seeded in a μ-dish (glass bottom, 35 mm, IBiDi) at a density of 100k cells per well 24 h before the microscopy measurement.

For imaging, the culture medium was removed and the cells were washed with Opti-MEM (Gibco-Invitrogen). Cells were stained with a Hoechst dye with a concentration of 5 μg mL^{-1} for 15 min at 37°C. Then cells were washed again with Opti-MEM and a freshly prepared suspension of NPs (with a concentration of 0.004 g L^{-1}) in Opti-MEM was added to the cells and incubated for 30 min at 37°C. Finally, cells were washed once again with Opti-MEM and imaged.

Cytotoxicity studies were performed by seeding HeLa cells in 96-well plates with a concentration of ∼10k cells per well in 100 μL of the DMEM growth medium and incubating them overnight. Then NPs were added by replacing the DMEM with the same culture medium containing increasing quantities of nanoparticles. Cells were incubated for 24 h in the presence of NPs, then the culture medium was removed and the wells washed with PBS. The wells were filled with DMEM containing MTT (3-(4,5-dimethylthiazol-2-yl)-2,5-diphenyltetrazolium bromide), and the cells were again incubated at 37°C for 4 h. The formazan crystals were redissolved by adding 100 μL of DMSO and shaking gently for 10 min. Then the absorbance at 570 nm on each well was read with a microplate reader. Experiments were carried out in triplicates, and the viability of the cells is expressed as a percentage of viable cells compared to the control group.

ACKNOWLEDGMENTS

This work was supported by the European Research Council ERC Consolidator grant BrightSens 648528. We thank C. Crucifix from the FRISBI platform for help with the electron microscopy.

ETHICS STATEMENT

There are no ethical issues in this work.

CONFLICT OF INTEREST

The authors declare no conflict of interest.

DATA AVAILABILITY STATEMENT

The data that support the findings of this study are available from the corresponding author upon reasonable request.

ORCID

Andrey S. Klymchenko https://orcid.org/0000-0002-2423-830X

REFERENCES

1. O. S. Wolfbeis, *Chem. Soc. Rev.* **2015**, *44*, 4743.
2. S. S. Kelkar, T. M. Reineke, *Bioconjug. Chem.* **2011**, *22*, 1879.
3. J. Qian, B. Z. Tang, *Chem* **2017**, *3*, 56.
4. P. D. Howes, R. Chandrawati, M. M. Stevens, *Science* **2014**, *346*, 53.
5. X. Michalet, *Science* **2005**, *307*, 538.
6. N. Hildebrandt, C. M. Spillmann, W. R. Algar, T. Pons, M. H. Stewart, E. Oh, K. Susumu, S. A. Díaz, J. B. Delehanty, I. L. Medintz, *Chem. Rev.* **2017**, *117*, 536.
7. M. Montalti, L. Prodi, E. Rampazzo, N. Zaccheroni, *Chem. Soc. Rev.* **2014**, *43*, 4243.
8. P. G. Luo, S. Sahu, S. - T. Yang, S. K. Sonkar, J. Wang, H. Wang, G. E. LeCroy, L. Cao, Y. - P. Sun, *J. Mater. Chem. B* **2013**, *1*, 2116.
9. V. N. Mochalin, O. Shenderova, D. Ho, Y. Gogotsi, *Nat. Nanotechnol.* **2012**, *7*, 11.
10. H. - S. Peng, D. T. Chiu, *Chem. Soc. Rev.* **2015**, *44*, 4699.
11. Y. Chen, J. W. Y. Lam, R. T. K. Kwok, B. Liu, B. Z. Tang, *Mater. Horizons* **2019**, *6*, 428.
12. Y. Li, S. Liu, H. Ni, H. Zhang, H. Zhang, C. Chuah, C. Ma, K. S. Wong, J. W. Y. Lam, R. T. K. Kwok, J. Qian, X. Lu, B. Z. Tang, *Angew. Chem. Int. Ed.* **2020**, *59*, 12822.
13. J. Mei, N. L. C. Leung, R. T. K. Kwok, J. W. Y. Lam, B. Z. Tang, *Chem. Rev.* **2015**, *115*, 11718.
14. C. Wu, D. T. Chiu, *Angew. Chem., Int. Ed.* **2013**, *52*, 3086.
15. J. Pecher, S. Mecking, *Chem. Rev.* **2010**, *110*, 6260.
16. A. S. Klymchenko, F. Liu, M. Collot, N. Anton, *Adv. Healthcare Mater.* **2021**, *10*, 2001289.
17. K. Li, B. Liu, *Chem. Soc. Rev.* **2014**, *43*, 6570.
18. A. Reisch, A. S. Klymchenko, *Small* **2016**, *12*, 1968.
19. S. Y. Ong, C. Zhang, D. Xiao, S. Q. Yao, *Angew. Chem., Int. Ed.* **2021**, 60, 17797. https://doi.org/10.1002/anie.202101964.

20. B. Andreiuk, A. Reisch, M. Lindecker, G. Follain, N. Peyriéras, J. G. Goetz, A. S. Klymchenko, *Small* **2017**, *13* (38), 1701582.
21. A. Reisch, P. Didier, L. Richert, S. Oncul, Y. Arntz, Y. Mély, A. S. Klymchenko, *Nat. Commun.* **2014**, *5*, 4089.
22. K. Trofymchuk, A. Reisch, I. Shulov, Y. Mély, A. S. Klymchenko, *Nanoscale* **2014**, *6*, 12934.
23. A. Wagh, S. Y. Qian, B. Law, *Bioconjug. Chem.* **2012**, *23*, 981.
24. A. Wagh, F. Jyoti, S. Mallik, S. Qian, E. Leclerc, B. Law, *Small* **2013**, *9*, 2129.
25. X. Zhang, K. Wang, M. Liu, X. Zhang, L. Tao, Y. Chen, Y. Wei, *Nanoscale* **2015**, *7*, 11486.
26. J. Geng, K. Li, W. Qin, L. Ma, G. G. Gurzadyan, B. Z. Tang, B. Liu, *Small* **2013**, *9*, 2012.
27. C. Grazon, J. Rieger, R. Méallet-Renault, B. Charleux, G. Clavier, *Macromolecules* **2013**, *46*, 5167.
28. Z. Tian, A. D. Shaller, A. D. Q. Li, *Chem. Commun.* **2009**, 180. https://doi.org/10.1039/B815507K
29. B. Zhang, H. Soleimaninejad, D. J. Jones, J. M. White, K. P. Ghiggino, T. A. Smith, W. W. H Wong, *Chem. Mater.* **2017**, *29*, 8395.
30. B. Andreiuk, A. Reisch, E. Bernhardt, A. S. Klymchenko, *Chem. - Asian J.* **2019**, *14*(6), 836.
31. I. Krossing, I. Raabe, *Angew. Chem., Int. Ed.* **2004**, *43*, 2066.
32. M. Jia, M. Bandini, *ACS Catal.* **2015**, *5*, 1638.
33. W. E. Geiger, F. Barrière, *Acc. Chem. Res.* **2010**, *43*, 1030.
34. A. B. A. Rupp, I. Krossing, *Acc. Chem. Res.* **2015**, *48*, 2537.
35. I. Raabe, K. Wagner, K. Guttsche, M. Wang, M. Grätzel, G. Santiso-Quiñones, I. Krossing, *Chem. Eur. J.* **2009**, *15*, 1966.
36. A. Rupp, N. Roznyatovskaya, H. Scherer, W. Beichel, P. Klose, C. Sturm, A. Hoffmann, J. Tübke, T. Koslowski, I. Krossing, *Chem. Eur. J.* **2014**, *20*, 9794.
37. X. Xie, A. Gutiérrez, V. Trofimov, I. Szilagyi, T. Soldati, E. Bakker, *Anal. Chem.* **2015**, *87*, 9954.
38. D. Ma, L. Duan, Y. Qiu, *J. Mater. Chem. C* **2016**, *4*, 5051.
39. I. Shulov, Y. Arntz, Y. Mély, V. G. Pivovarenko, A. S. Klymchenko, *Chem. Commun.* **2016**, *52*, 7962.
40. H. Yao, K. Ashiba, *RSC Adv*. **2011**, *1*, 834.
41. D. K. Bwambok, B. El-Zahab, S. K. Challa, M. Li, L. Chandler, G. A. Baker, I. M. Warner, *ACS Nano* **2009**, *3*, 3854.
42. I. Shulov, S. Oncul, A. Reisch, Y. Arntz, M. Collot, Y. Mely, A. S. Klymchenko, *Nanoscale* **2015**, *7*, 18198.
43. I. O. Aparin, N. Melnychuk, A. S. Klymchenko, *Adv. Opt. Mater.* **2020**, *8*, 2000027.
44. B. Andreiuk, A. Reisch, V. G. Pivovarenko, A. S. Klymchenko, *Mater. Chem. Front.* **2017**, *1*, 2309.
45. C. R. Benson, L. Kacenauskaite, K. L. VanDenburgh, W. Zhao, B. Qiao, T. Sadhukhan, M. Pink, J. S. Chen, S. Borgi, C. H. Chen , B J. Davis, Y. C. Simon, K. Raghavachari, B W. Laursen, A. H. Flood, *Chem* **2020**, *6*, 1978.
46. C. Severi, N. Melnychuk, A. S. Klymchenko, *Biosens. Bioelectron.* **2020**, 168.
47. P. Ashokkumar, N. Adarsh, A. S. Klymchenko, *Small* **2020**, *16*, 2002494.
48. A. Reisch, K. Trofymchuk, A. Runser, G. Fleith, M. Rawiso, A. S. Klymchenko, *ACS Appl. Mater. Interfaces* **2017**, *9*, 43030.
49. N. Melnychuk, A. S. Klymchenko, *J. Am. Chem. Soc.* **2018**, *140*, 10856.
50. A. Reisch, D. Heimburger, P. Ernst, A. Runser, P. Didier, D. Dujardin, A. S. Klymchenko, *Adv. Funct. Mater.* **2018**, *28*, 1805157.
51. S. Egloff, A. Runser, A. Klymchenko, A. Reisch, *Small Methods* **2021**, *5*, 2000947.
52. I. Khalin, D. Heimburger, N. Melnychuk, M. Collot, B. Groschup, F. Hellal, A. Reisch, N. Plesnila, A. S. Klymchenko, *ACS Nano* **2020**, *14*, 9755.
53. K. Trofymchuk, A. Reisch, P. Didier, F. Fras, P. Gilliot, Y. Mely, A. S. Klymchenko, *Nat. Photonics* **2017**, *11*, 657.
54. S. Egloff, N. Melnychuk, A. Reisch, S. Martin, A. S. Klymchenko, *Biosens. Bioelectron.* **2021**, 179.
55. N. Melnychuk, S. Egloff, A. Runser, A. Reisch, A. S. Klymchenko, *Angew. Chem. Int. Ed.* **2020**, *59*, 6811.
56. G. Bao, S. Wen, G. Lin, J. Yuan, J. Lin, K. - L. Wong, J.-C. G. Bünzli, D. Jin, *Coord. Chem. Rev.* **2021**, *429*, 213642.
57. H. Liang, Z. Hong, S. Li, X. Song, D. Zhang, Q. Chen, J. Li, H. Yang, *Adv. Funct. Mater.* **2021**, 31(5), 2006353.
58. H. Guo, X. Song, W. Lei, C. He, W. You, Q. Lin, S. Zhou, X. Chen, Z. Chen, *Angew. Chem. Int. Ed.* **2019**, *58*, 12195.
59. L. Armelao, S. Quici, F. Barigelletti, G. Accorsi, G. Bottaro, M. Cavazzini, E. Tondello, *Coord. Chem. Rev.* **2010**, *254*, 487.
60. J.-C. G. Bünzli, *Chem. Rev.* **2010**, *110*, 2729.
61. S. V. Eliseeva, J. C. G. Bunzli, *Chem. Soc. Rev.* **2010**, *39*, 189.
62. A. K. Hagan, T. Zuchner, *Anal. Bioanal. Chem.* **2011**, *400*, 2847.
63. X. H. Wang, H. J. Chang, J. Xie, B. Z. Zhao, B. T. Liu, S. L. Xu, W. B. Pei, N. Ren, L. Huang, W. Huang, *Coord. Chem. Rev.* **2014**, *273*, 201.
64. J. Vuojola, T. Soukka, *Methods and Appl. Fluoresc.* **2014**, *2*(1), 012001.
65. M. Cardoso Dos Santos, A. Runser, H. Bartenlian, A. M. Nonat, L. J. Charbonnière, A. S. Klymchenko, N. Hildebrandt, A. Reisch, *Chem. Mater.* **2019**, *31*, 4034.
66. D. B. A. Raj, S. Biju, M. L. P Reddy, *Inorg. Chem.* **2008**, *47*, 8091.
67. A. Reisch, A. Runser, Y. Arntz, Y. Mély, A. S. Klymchenko, *ACS Nano* **2015**, *9*, 5104.
68. E. B. Sveshnikova, S. S. Dudar, V. L. Ermolaev, *Opt. Spectrosc.* **2006**, *100*, 840.
69. H. D. B. Jenkins, K. P. Thakur, *J. Chem. Educ.* **1979**, *56*, 576.
70. R. Weissleder. *Nat. Biotechnol.* **2001**, *19*, 316.
71. L. Yuan, W. Lin, K. Zheng, L. He, W. Huang. *Chem. Soc. Rev.* **2013**, *42*, 622.
72. P. Müller, P. Schwille, T. Weidemann, *Bioinformatics* **2014**, *30*, 2532.
73. C. Würth, M. Grabolle, J. Pauli, M. Spieles, U. Resch-Genger, *Nat. Protoc.* **2013**, *8*, 1535.
74. A. M. Brouwer. *Pure Appl. Chem.* **2011**, *83*, 2213.

SUPPORTING INFORMATION

Additional supporting information may be found in the online version of the article at the publisher's website.

How to cite this article: C. Severi, S. Lahtinen, J. Rosenberg, A. Reisch, T. Soukka, A. S. Klymchenko. *Aggregate*. **2021**, e130. https://doi.org/10.1002/agt2.130